ACS NANO

www.acsnano.org

ARTICLE

Controlling Chiroptical Responses via Chemo-Mechanical Deformation of DNA Origami Structures

Taehwi Kim, Chanseok Lee, Jae Young Lee, and Do-Nyun Kim*

Cite This: *ACS Nano* 2024, 18, 3414–3423

Read Online

ACCESS | Metrics & More | Article Recommendations | Supporting Information

ABSTRACT: **DNA origami-based templates have been widely used to fabricate chiral plasmonic metamaterials due to their precise control of the placement of nanoparticles (NPs) in a desired configuration. However, achieving various chiroptical responses inevitably requires a change in the structure of DNA origami-based templates or binding sites on them, leading to the use of significantly different sets of DNA strands. Here, we propose an approach to controlling various chiroptical responses with a single DNA origami design using its chemo-mechanical deformation induced by DNA intercalators. The chiroptical response could be finely tuned by altering the concentration of intercalators only. The silver (Ag) enhancement was used to amplify the chiroptical signal by enlarging NPs and to maintain it by stiffening the template DNA structure. Furthermore, the sensitivity in the chiroptical signal change to the concentration of intercalators could be modulated by the type of intercalator, the mixture of two intercalators, and the stiffness of DNA origami structures. This approach would be useful in a variety of optical applications that require programmed spatial modification of chiroptical responses.**

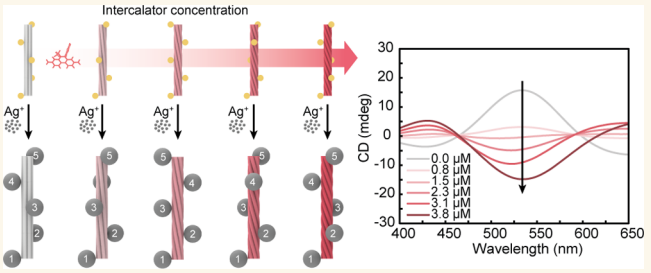

KEYWORDS: *chiroptical response, plasmonic nanoparticles, DNA nanotechnology, intercalator, Ag enhancement, circular dichroism*

Chiral plasmonic metamaterials exhibit chiroptical activity due to their characteristics of surface plasmon resonance and chirality. Since chiral structures do not overlap with their mirror image, chiral-shaped plasmonic metamaterials have different responses to left- or right-circularly polarized light. If constructed at the nanoscale, they can interact with visible light, which is highly useful in various applications.[1] While several methods have been studied for realizing chiral shapes including direct laser lithography,[2] glancing angle deposition,[3] and directed synthesis,[4] they often require fine-tuning of manufacturing conditions, rendering it difficult to build a complex shape at the nanoscale. Alternatively, more easily accessible achiral plasmonic NPs such as gold nanoparticles (AuNPs) and gold nanorods can be used. Although they do not show chiroptical activity individually, it can be achieved by the chiral arrangement of these particles in close proximity due to plasmon coupling between them. For example, the twist or stacking angle of a polymer substrate with NPs was directly controlled.[5,6] Furthermore, diverse types of chiral templates such as polymer,[7] nanofiber,[8] liquid crystal,[9] and peptide[10,11] have been employed for the attachment of NPs in the chiral form.

DNA origami[12] is a promising template where achiral plasmonic NPs can be precisely arranged in nanometer resolution. Its high programmability has enabled the reliable construction of nanostructures in arbitrary shapes by folding a long DNA strand with multiple short strands of rationally designed sequences. Precise control over the arrangement of plasmonic NPs on DNA origami nanostructures has been successfully demonstrated.[1,13−15] Its dynamic change through the reconfiguration of DNA origami induced by strand displacement reactions[16−22] and environmental stimuli[23−30] have been shown to be possible.

However, controlling chiroptical responses with these conventional methods remains limited. For example, although they can be varied by designing the locations where NPs bind the structure, they are highly limited due to the helical nature of the DNA duplex, which inevitably restricts the position where DNA handle strands can point outward for the attachment of NPs. The twist of the DNA structure itself

Received: October 23, 2023
Revised: January 11, 2024
Accepted: January 12, 2024
Published: January 18, 2024

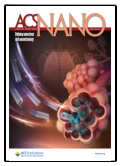

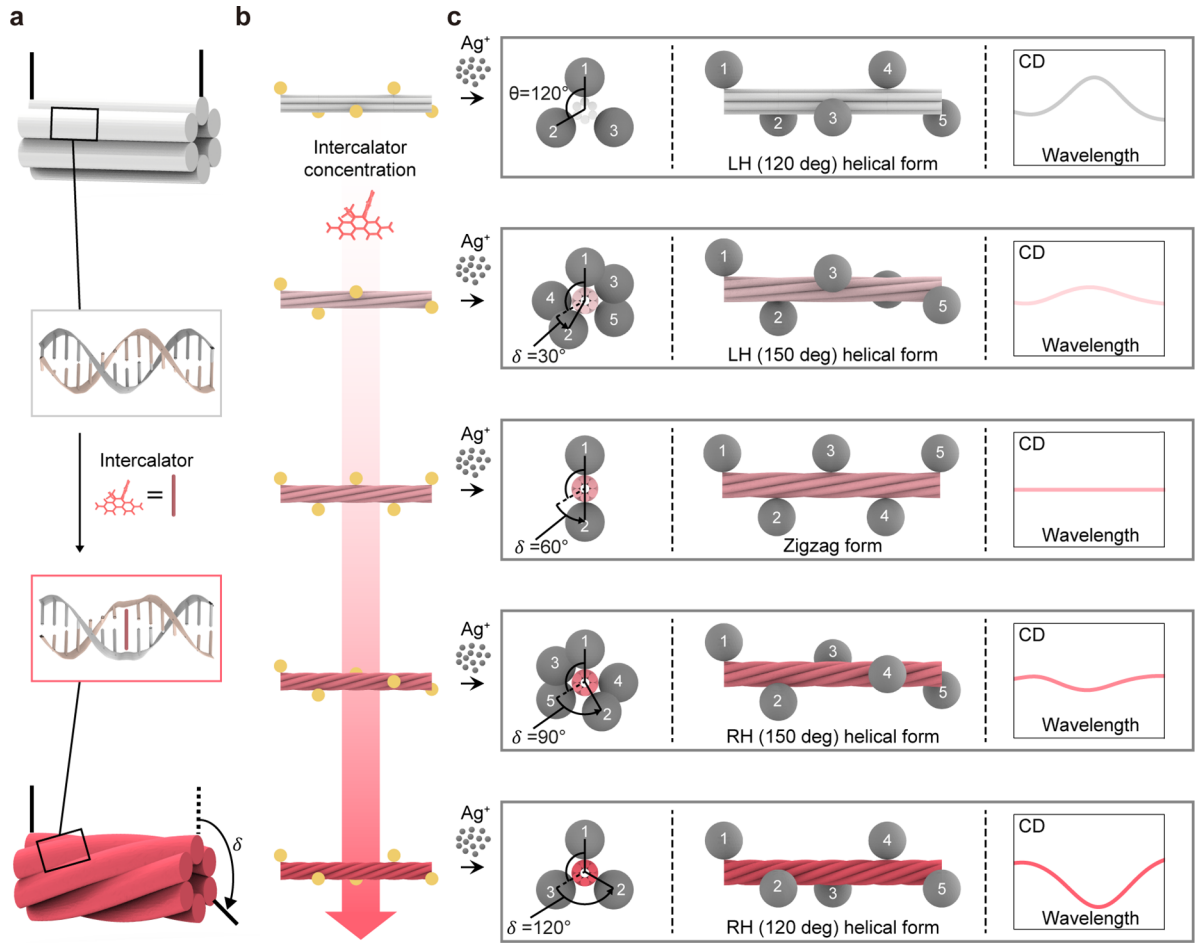

Figure 1. Principle of controlling the chiroptical response. (a) Torsional deformation of a unit block in 6HB due to the unwinding effect of an intercalator. (b) Various NP arrangements dependent on the concentration of intercalators. (c) Corresponding CD signals after Ag enhancement. θ is the initial angle between neighboring AuNPs without intercalators. δ is the twist angle per unit block between adjacent NPs. Bold straight lines indicate the ideal positions and orientations of the first and second NPs. Dotted straight lines indicate the initial position of the second NP. The degree in parentheses represents the acute angle in the axial direction between adjacent NPs.

can be finely tuned,[31] but in this case, we need different sets of constituent DNA strands to construct each structure with different twists, which is costly and inefficient to realize diverse chiroptical responses. Alternatively, several methods to control the chiroptical signal dynamically have been proposed.[16−30] Their structures (and hence the attached NPs) were switching between a few configurationally restricted (*e.g.*, open and closed) states only by using a rather simple on-and-off mechanism controlled by the stimuli-responsive formation of double-stranded DNA (dsDNA). As a result, while it was possible to obtain continuously varying chiroptical signals, accurate control over a wide range of them was challenging due to the difficulty in the adjustment of the ratio between these restricted states.[23−30]

Here, we propose a way of controlling the chiroptical response with a single DNA origami design using the chemo-mechanical deformation induced by DNA intercalators. The unwinding of dsDNA, when intercalators bind, is used to induce the torsional deformation of the DNA origami structure, which modulates, in turn, the NP arrangement on it. Various chiroptical responses could be obtained conveniently by changing the concentrations of intercalators only. The sensitivity in the chiroptical signal change to the concentration of intercalators could be tuned by using different types of intercalators or their mixtures and by changing the stiffness of DNA origami structures. We used the Ag enhancement to amplify the designated signal by enlarging NPs[1] and to maintain it by stiffening the template DNA structure[32−34] even after the change in the concentration of intercalators. This ability to realize various chiroptical responses would be useful in applications such as optical metasurfaces, where a programmable spatial variation of chiroptical responses is necessary.

RESULTS AND DISCUSSION

Design and Principle. DNA intercalators change the equilibrium configuration of dsDNA when bound. For example, ethidium bromide (EtBr) is known to unwind unconstrained dsDNA so that its helical pitch increases from 10.5 base pairs (bp) per turn for B-form DNA.[35,36] These chemicals may induce mechanical stresses into structured DNA assemblies because DNA helices on them are cross-linked and constrained by Holliday junctions (crossovers), thereby deforming the structure into bent and/or twisted shapes.[37,38]

Here, we propose to use this chemo-mechanical deformation for controlling the chiroptical response. To illustrate, we constructed an initially straight six-helix bundle (6HB) on the

https://doi.org/10.1021/acsnano.3c10386
ACS Nano 2024, 18, 3414−3423

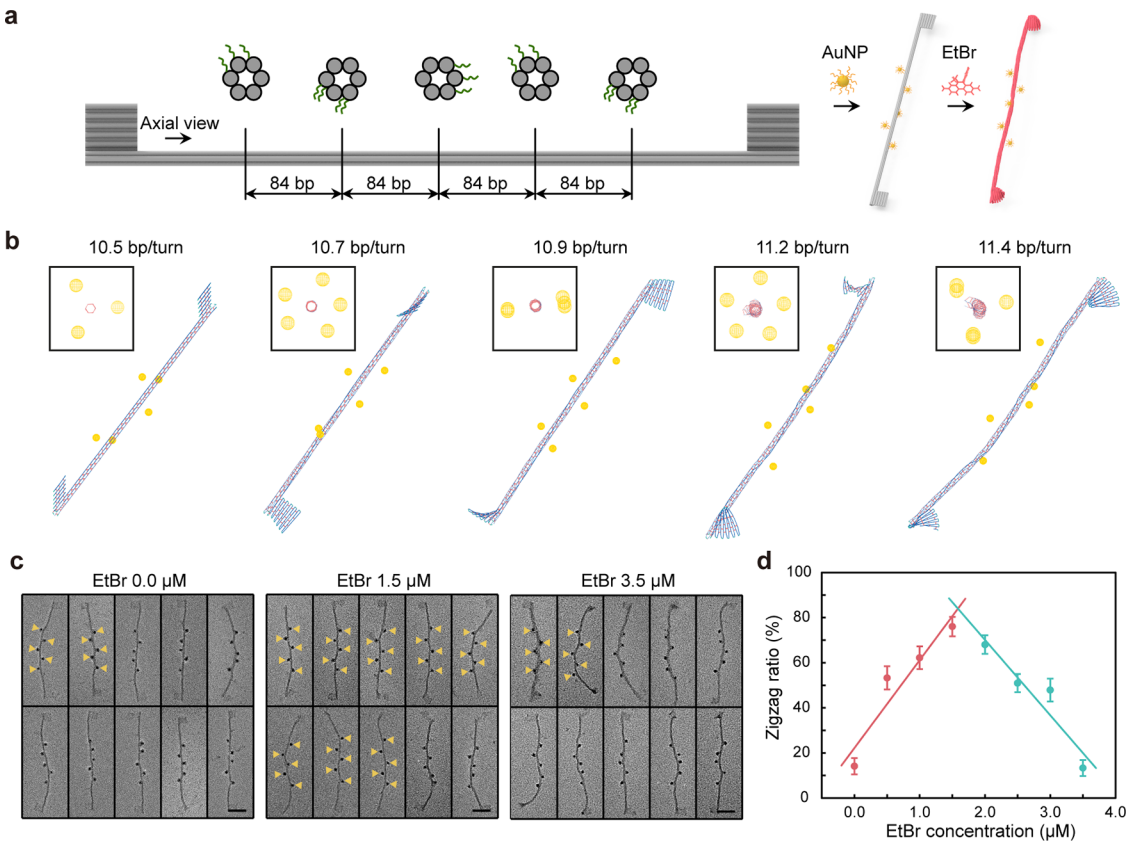

Figure 2. Prediction and characterization for AuNP arrangements. (a) 6HB design with the protruding DNA handles for the attachment of AuNPs and process of attaching AuNPs and adding intercalators. (b) Predicted arrangements of AuNPs with respect to the helical pitch using the SNUPI analysis. Images in squares show the AuNP arrangement in the axial view. (c) TEM images showing deposition forms of AuNPs depending on the EtBr concentration. Yellow triangles indicate the positions of AuNPs in the zigzag deposition form. Scale bars are 50 nm. (d) Ratio of AuNPs in the zigzag deposition form dependent on the EtBr concentration. Error bars were obtained using the bootstrapping method. Specific numbers are shown in Figure S4. Solid straight lines were obtained by linear regression.

honeycomb lattice designed to exhibit a torsional deformation in the left-handed (LH) direction via the unwinding effect of intercalators (Figure 1a). Its twist angle per unit block (δ) would increase monotonically with the concentration of intercalators until saturated. The positions of protruded DNA handles for AuNP attachment were designed so as to locate five AuNPs with LH helical form at an equal distance on the straight bundle ($\delta = 0°$) consisting of four unit blocks (Figure 1b). The initial angle θ between neighboring AuNPs without intercalators was set to approximately 120°. The torsional deformation of the bundle would increase continuously with the concentration of intercalators, which would, in turn, change the AuNP arrangement on it gradually. For example, if δ is increased to 60°, the angle between the adjacent AuNPs becomes 180°, ideally leading to the zigzag form having achiral properties. If δ is further increased to 120°, AuNPs show the right-handed (RH) helical form opposite to their initial one. Note that while intercalators induce monotonic torsional deformation in the LH direction to DNA origami bundles, various chiroptical responses can be achieved through the rational design of the initial arrangement for discretely attached AuNPs. The Ag enhancement was employed to increase the size of AuNPs large enough to get the chiroptical signal (Figure 1c). It also stiffened the template DNA structure[32−34] so that its deformed shape hardly changed with the concentration of intercalators maintaining the designated chiroptical signal.

Characterization of AuNP Arrangements. For quantitative characterization of AuNP arrangements, we used 6HB with additional flag-like regions at its ends,[31,35] which assist the observation of torsional deformation of the bundle (Figure 2a and Figure S1). From the middle of the bundle, five AuNPs were attached with three or four DNA handle strands per binding site at 84 bp and 120° intervals along the axial axis to set the AuNP arrangement on the template bundle initially to the LH helical form. Then, EtBr at various concentrations was introduced as the intercalator to induce the torsional deformation of the bundle and the corresponding change in the chirality of the AuNP arrangements.

We first simulated the AuNP arrangement induced by the chemo-mechanical deformation of 6HB using SNUPI[39,40] (Figure 2b). The unwinding effect dependent on the concentration of intercalators was modeled by increasing the helical pitch from the reference value (10.5 bp per turn). When we calculated the final positions of AuNPs on 6HB from the SNUPI analysis results (Note S1), the initial form of AuNP arrangement (set to 120° intervals per 84 bp) was found to be crucial to achieving states gradually varying from LH to achiral to RH helical forms according to the change in the helical pitch (Figure S2). The achiral zigzag form was observed around the helical pitch of 10.9 bp per turn, and the RH helical form appeared at the helical pitch of approximately 11.4 bp per turn. These results indicated that various chiral properties of AuNP

https://doi.org/10.1021/acsnano.3c10386
ACS Nano 2024, 18, 3414−3423

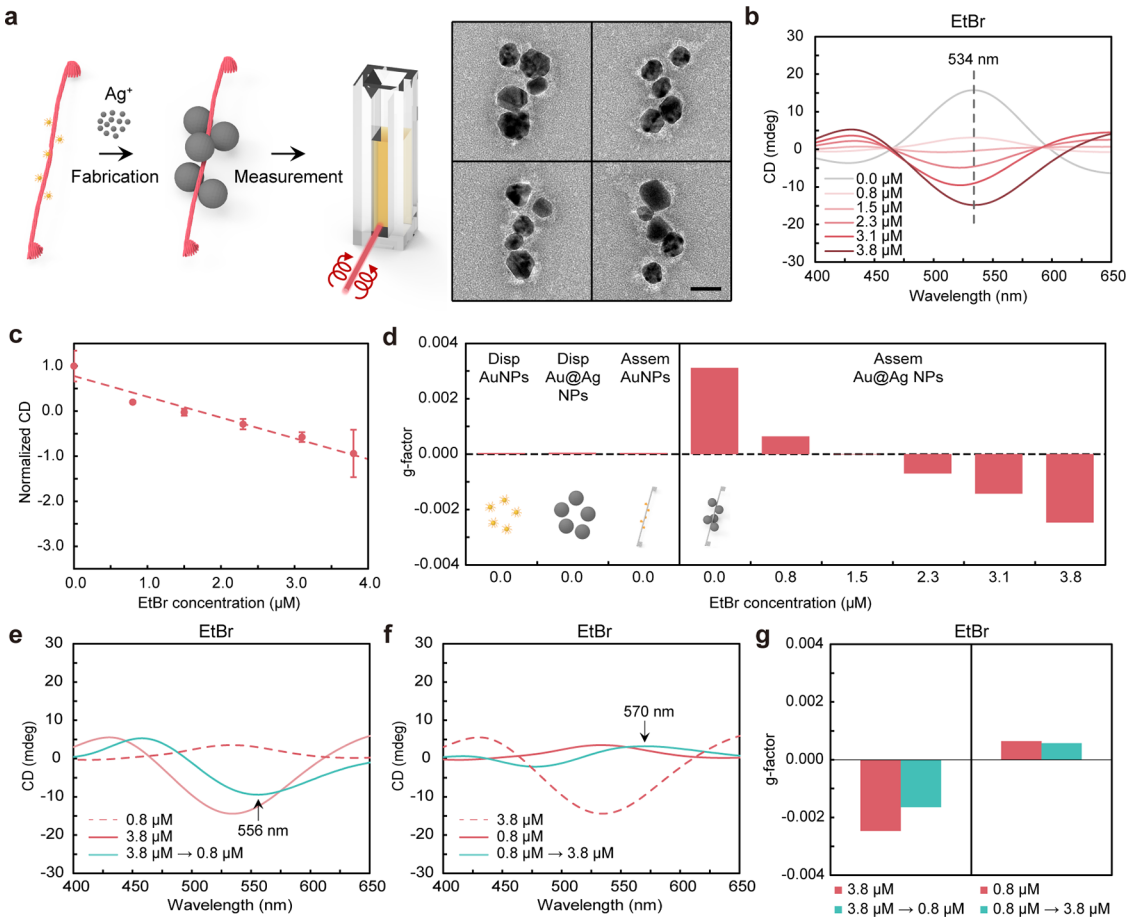

Figure 3. Ag enhancement. (a) Fabrication stage with Ag enhancement and measurement stage of increasing total volume to measure the CD signals. TEM images show the arrangement of Au@Ag NPs at zero EtBr concentration. Scale bar is 50 nm. (b) Measured CD spectra for various EtBr concentrations. The peak wavelength without EtBr is 534 nm, as indicated by the dotted line. (c) Normalized CD values at 534 nm for different EtBr concentrations. Dashed straight lines were obtained by linear regression. (d) The g-factors for various conditions of NPs (dispersed AuNPs, dispersed Au@Ag NPs, assembled AuNPs, assembled Au@Ag NPs, and modified assemblies of Au@Ag NPs dependent on EtBr concentration). (e and f) CD spectra in the change of EtBr concentration after Ag enhancement. Arrows indicate the dip and peak wavelengths for each spectrum. (g) Comparison of g-factors for the changed and unchanged EtBr concentrations during the measurement stage. Those for the change in EtBr concentration were obtained at the indicated dip and peak wavelength, respectively.

arrangements would be possible by adding intercalators to change the effective helical pitch of dsDNA.[35,36]

For experimental verification, AuNPs of 5 nm diameters were attached to five binding sites on 6HB. The yield of attaching five AuNPs to the 6HB was roughly ~80% when we counted the number of AuNPs from the atomic force microscopy (AFM) images (Figure S3). We measured the zigzag ratio at various EtBr concentrations by using transmission electron microscopy (TEM) on negative-stained samples. It was defined as the number of bundles with the zigzag deposition form of AuNPs divided by the total number of bundles (Figures 2c, 2d, and S4). Ideally, it would be zero if the AuNP arrangement would be either the LH or RH helical form, while it would be one for the fully zigzag form. In practice, due to the flexibility of the bundle and its handle strands for AuNP attachment, 14.1% of bundles showed the zigzag deposition form of AuNPs even without EtBr. However, as the concentration of EtBr increased, the zigzag ratio monotonically increased and reached its maximum value of 76.0% at approximately 1.5 μM, where two-dimensional zigzag forms were dominant. Then, it decreased and reached its minimum value of 13.3% around 3.5 μM EtBr as the RH helical form of AuNPs became dominant. These results illustrated that the AuNP arrangement could be successfully varied with intercalators, inducing torsional deformation of the template DNA origami bundle.

Ag Enhancement. We employed Ag ions to amplify the designated chiroptical signal by enlarging AuNPs and to maintain it even after a change in the concentration of intercalators by stiffening the template DNA bundle. First of all, the diameter of ~5 nm for the original AuNPs and the gap of ~25 nm between them were not suitable to achieve plasmon coupling for chiroptical activity (Figures S5 and S6). Hence, we enlarged the diameter of NPs from ~5 to ~38 nm and reduced the gap between them from ~25 to ~2 nm on average via Ag enhancement[1,41] (Figure 3a and Figure S7). The structures were then diluted under the same buffer condition to fill a cuvette for circular dichroism (CD) measurements (Figure 3a). Without the addition of EtBr, the CD signal exhibited a characteristic bisignate peak−dip shape with its peak value of 15.8 mdeg at a wavelength of 534 nm (Figure 3b and Figure S8), indicating the LH helical form of Au@Ag NP arrangements. The peak value decreased with the concentration of EtBr and the CD spectra became almost flat at 1.5 μM, corresponding to the achiral zigzag form of Au@Ag NP arrangements (Figure 3b and Figure S9). Further addition of

https://doi.org/10.1021/acsnano.3c10386
ACS Nano 2024, 18, 3414−3423

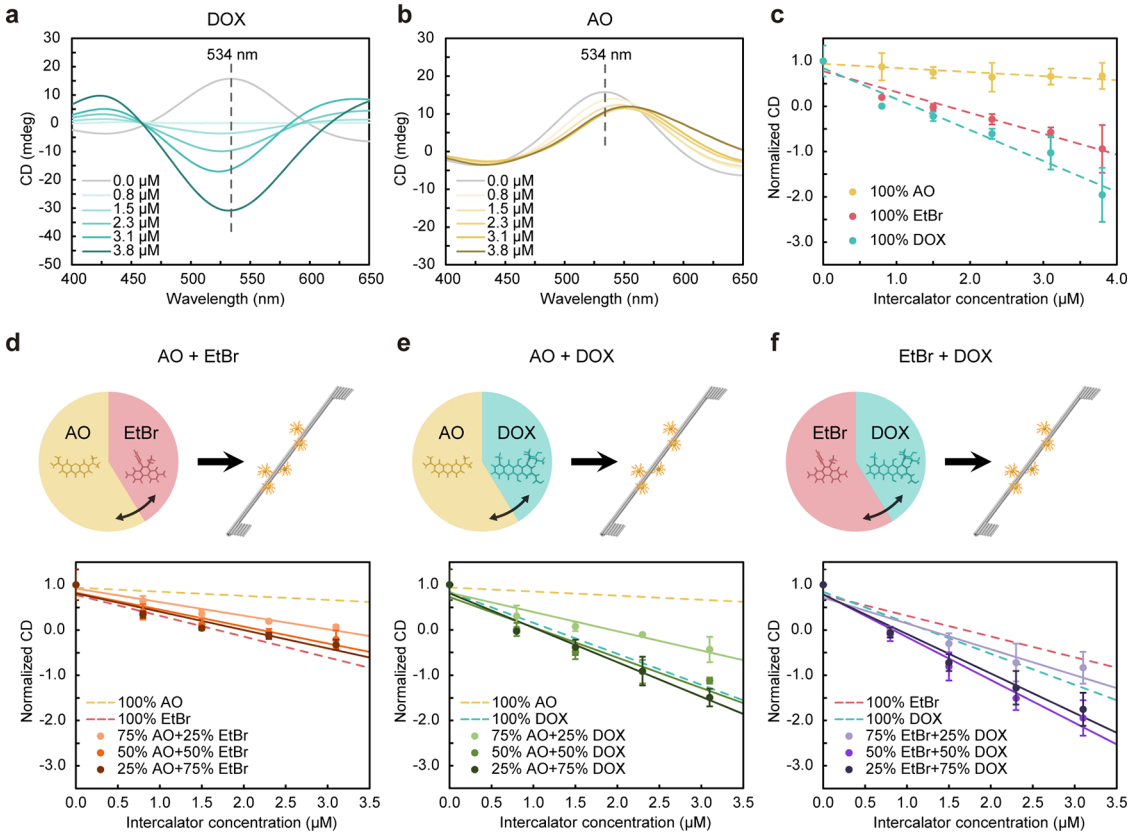

Figure 4. Sensitivity of chiroptical response change depending on the type and combination of intercalators. (a and b) CD spectra when DOX and AO were used as the intercalator. (c–f) Normalized CD values at 534 nm for three intercalators (EtBr, DOX, and AO) and their mixtures. Dashed and solid straight lines in c–f were obtained by linear regression.

EtBr led to the increase of the peak CD signal in the opposite direction, resulting in a fully reversed CD spectrum around 3.8 μM due to the RH helical form of the Au@Ag NP arrangements. Normalized CD values at the wavelength of 534 nm showed almost linear dependency on the EtBr concentration (Figure 3c). We further calculated the g-factors at the wavelength of 534 nm to see the variation of chiroptical responses with respect to the EtBr concentration more clearly (Figure 3d and Figures S5 and S6). Those for dispersed AuNPs, dispersed Au@Ag NPs, and assembled AuNPs were considerably lower. These results confirmed that various chiroptical responses could be obtained effectively with the proposed, DNA-origami-templated Au@Ag NP system using DNA intercalators.

It has been reported that Ag ions bind and stiffen the DNA helices.[32−34] We used this effect to stabilize the designated chiroptical signal for the concentration change. To demonstrate it, we measured CD signals of two assemblies fabricated at 3.8 and 0.8 μM EtBr with Ag enhancement (Figures 3e, 3f, and S10). Both assemblies had similar CD spectra even after the change of EtBr concentration in the dilution for the CD measurement, suggesting that the designated chiroptical signal could be maintained to some extent. To compare this, we estimated g-factors at the dip and peak wavelengths for 3.8 and 0.8 μM, respectively (Figure 3g). The g-factors remained constant despite the change in EtBr concentration. The redshift might be caused by the electrostatic screening effect of bound Ag ions reducing the repulsive forces between DNA helices.[42,43] As a result, DNA helices in the structure became more densely packed, leading to a decrease in the distance between Au@Ag NPs. This reduction in the distance between Au@Ag NPs might be responsible for the observed redshift.[11] It could also be observed when we increased the concentration of $MgCl_2$ having a similar screening effect (Figure S11). Except for this unwanted effect, the desired chiroptical signal could be stabilized for the change in the concentration of intercalators effectively by Ag enhancement.

Type and Combination of Intercalators. The torsional deformation of DNA origami bundles would vary with the intercalator type because each intercalator has a different unwinding angle per molecule and binding affinity. As a result, the sensitivity in the chiroptical response change to the concentration of intercalators would be dependent on their type. To investigate, we tested two additional intercalators, doxorubicin (DOX) and acridine orange (AO), and measured the CD signals at various intercalator concentrations (Figures 4a–4c and Figures S12 and S13). DOX resulted in similar CD spectra but exerted a stronger chemo-mechanical effect than EtBr. The peak CD at 534 nm dropped to −30.4 mdeg when 3.8 μM DOX was added, approximately 2 times more than that observed with the addition of the same amount of EtBr. In contrast, CD values barely changed with AO. The peak CD dropped to 10.6 mdeg even with 3.8 μM AO. Nevertheless, a redshift appeared in the CD spectra probably due to the reduction in the distance between NPs.[11,42,43] It has been reported for the interaction of AO with DNA that intercalation is dominant at a low concentration and electrostatic binding becomes more prominent as the concentration of AO increases.[44] Hence, the repulsive electrostatic forces between DNA helices might decrease with the AO concentration,

https://doi.org/10.1021/acsnano.3c10386
ACS Nano 2024, 18, 3414−3423

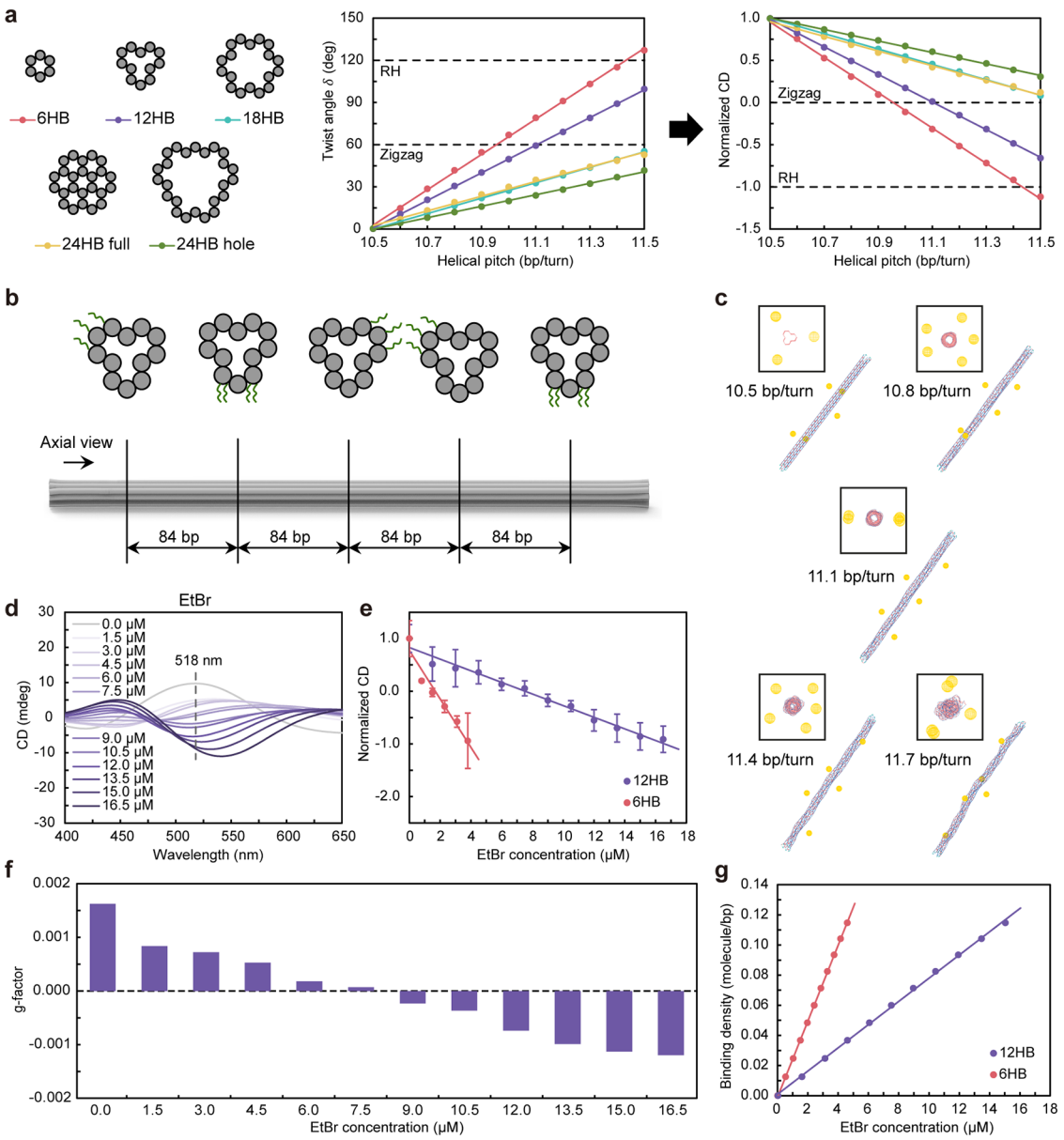

Figure 5. Sensitivity of chiroptical response change depending on the stiffness of DNA origami bundles. (a) Five representative cross-sectional shapes of DNA origami bundles. Dependence of δ and the normalized CD on the helical pitch for different cross-sectional shapes. (b) 12HB design with the protruding DNA handles for the attachment of AuNPs. (c) Predicted arrangements of AuNPs at 12HB with respect to the helical pitch using the SNUPI analysis. Images in squares show the arrangement of AuNPs in the axial view. (d) CD spectra of Au@Ag NPs at 12HB measured for various EtBr concentrations. The peak wavelength at zero EtBr concentration is 518 nm. (e) Comparison of normalized CD values for Au@Ag NPs at 6HB and 12HB. Those at 12HB are normalized at 518 nm. (f) The g-factors at 12HB depending on EtBr concentration. They were obtained at 518 nm. (g) Estimated binding densities of EtBr with respect to its concentration (Figure S29). Solid straight lines in parts a−g were obtained by linear regression.

leading to a reduction in the effective diameter of DNA bundles and hence the distance between NPs. The slopes of the normalized peak CD to the intercalator concentration were −0.68, −0.46, and −0.09 μM^{-1} for DOX, EtBr, and AO, respectively. Consequently, the sensitivity to the concentration of intercalators is greater in the order of DOX, EtBr, and AO. Although the unwinding angle per molecule of EtBr (~26°)[45] was known to be the largest compared with that of AO (~17°)[46] and DOX (~11°),[47,48] the order of sensitivity was changed because the binding affinity of DOX was reported to be about 40 and 200 times larger than that of EtBr and AO, respectively, in the ionic strength of ~0.06 M,[49−51] similar to our experimental condition of ~0.05 M.

In addition, we explored the variation of chiroptical responses when the two intercalators were used together as a mixture. CD signals were measured with three mixing ratios (25%−75%, 50%−50%, and 75%−25%) of two intercalators at the same total concentration for each combination of intercalator types (Figures 4d−4f). For mixtures of AO and EtBr (Figure 4d and Figures S14−S16), the normalized CD values lay between 100% AO and EtBr lines but leaned toward the 100% EtBr line more. This result suggests that EtBr might be more competitive in intercalation than AO. A similar result was observed when AO and DOX were used as a mixture (Figure 4e and Figures S17−S19), with a stronger dependency on the DOX concentration. Interestingly, if we used the

https://doi.org/10.1021/acsnano.3c10386
ACS Nano 2024, 18, 3414−3423

mixture of DOX and EtBr (Figure 4f and Figures S20−S22), much higher sensitivities were observed even when compared to the sensitivity achievable with 100% DOX. The maximum sensitivity was obtained with the mixture of 50% DOX and 50% EtBr, and it decreased when the ratio of DOX was further increased. This result suggests that there might exist a cooperative effect in binding to DNA when these two intercalators were used. The structural deformation of the DNA helices due to the binding of one intercalator type might increase the binding of the other. Additional studies using, for example, molecular dynamics simulations would be necessary to reveal the exact mechanism. The g-factors obtained at a wavelength of 534 nm for different intercalators and their combinations also showed similar trends (Figure S23). Taken altogether, the sensitivity of chiroptical responses can be finely controlled by using a mixture of intercalators even in broader ranges compared to when only a single type of intercalator is used.

Stiffness of DNA Origami Bundles. While the sensitivity in the chiroptical response change can be effectively modulated by DNA intercalators, it is determined by the unwinding rate and binding affinity of the intercalators available. Alternatively, it can also be controlled by the stiffness of DNA origami bundles, which has been shown to be finely tuned in a wide range via cross-sectional design and engineered defects.[31,37,52,53] For example, various rates of change in δ with respect to the helical pitch could be achieved by changing the cross-sectional shape of the bundle according to the SNUPI analysis. Then, various slopes of the normalized peak CD to the helical pitch were obtained by assuming linear dependence of δ to the normalized peak CD (Figure 5a and Note S2).

To verify the effect of the bundle stiffness, we designed a 12-helix bundle (12HB) with binding sites to locate five NPs with the LH helical form at an equal distance on the straight bundle (Figure 5b and Figure S24). The yield of attaching five AuNPs to 12HB was roughly ∼87% (Figure S25). SNUPI analysis suggested that the helical pitches around 11.1 and 11.7 bp per turn were required for 12HB to achieve the achiral zigzag and RH helical forms, respectively, which were higher than those for 6HB (Figure 5c).

We measured CD signals of the Au@Ag NPs on 12HB by increasing the concentration of EtBr to 16.5 μM (Figure 5d and Figures S26−S28). The peak wavelength was shifted to 518 nm because of a larger effective diameter of 12HB than 6HB resulting in the increased gap between Au@Ag NPs.[11] CD values at a wavelength of 518 nm decreased monotonically with EtBr. The CD spectra became almost flat at 7.5 μM and then reversed at 15.0 μM compared to the initial chiroptical response. A redshift of the reversed peak CD values at higher than 15.0 μM was observed probably because the shrunken inner space of 12HB induced by an excessive deformation might cause the change in the helical radius of NP arrangement. To clearly identify the variations in the CD signals, we obtained the normalized CD and g-factor at a 518 nm wavelength (Figures 5e and 5f). The slope of the normalized CD for 12HB was ∼4.2 times smaller than that for 6HB. It is, however, ∼1.3 times larger than that predicted by SNUPI analysis with helical pitch variation (Figure 5a). This difference suggests that it might be harder for intercalators to be intercalated into the helices of a stiffer bundle. In other words, the stiffness of DNA origami bundles may affect the binding density of intercalators for a given concentration. Based on this hypothesis, we estimated the binding density of intercalators as a function of their concentration for 6HB and 12HB using simulated and measured CD variations (Figure 5g and Figure S29). The rates of binding density with respect to the concentration of intercalators were calculated as 0.025 and 0.008 molecules per bp·μM for 6HB and 12HB, respectively.

CONCLUSION

The proposed method offers a way to control the chiroptical response. It exploited the chemo-mechanical deformation of DNA origami bundles induced by DNA intercalators to finely and broadly tune the chiroptical response. Ag enhancement was employed to amplify the designated chiroptical signal by enlarging NPs and to stabilize it for the change in the concentration of intercalators by stiffening the template DNA bundle. We could control the sensitivity in the chiroptical response change to the concentration of intercalators by using different intercalators since each intercalator has a different binding affinity and unwinding effect on the dsDNA. Interestingly, using a mixture of two intercalators extended the controllable range of sensitivity even beyond the inherent sensitivity of each intercalator. Designing the stiffness of the DNA origami bundle was also an effective alternative to using different intercalators for modulating the sensitivity. Our approach would advance the development of chiral metasurfaces that require different chiroptical responses depending on the region[54−56] if combined with top-down technologies for precisely positioning DNA origami structures on a surface.[57−60]

METHODS

Folding DNA Origami Bundles. We designed 6HB and 12HB using caDNAno software[61] (Figures S1 and S24 and Tables S1 and S2), where the 6HB design was slightly modified from the one in the previous paper[31] for our study. To fold the bundles, we prepared 100 μL of the folding solution containing 10 nM scaffold DNA (M13mp18, Guild BioSciences, www.guildbiosciences.com), 100 nM each staple strand (Bioneer, www.bioneer.co.kr), 20 mM $MgCl_2$, and 1x TAE (40 mM Tris-acetate, 1 mM EDTA, Sigma-Aldrich). It was heated to 80 °C at 1 °C/s and annealed from 80 to 65 °C at −0.5 °C per 2 min and from 65 to 25 °C at −0.5 °C per 30 min using the T100 Thermal Cycler (Bio-Rad).

The annealed solution was purified by a poly(ethylene glycol) (PEG) precipitation to remove excess staple strands.[62] We mixed 100 μL of the annealed solution, 650 μL of a FoB20 buffer (20 mM $MgCl_2$, 5 mM NaCl, 1x TAE) and 750 μL of a precipitation buffer (15% PEG-8000, 500 mM NaCl, 1x TAE) sequentially. The mixture was centrifuged at 20,000 rcf and 4 °C for 25 min using the 1730R microcentrifuge (LaboGene). Its supernatant was carefully removed until 30 μL of the mixture remained. To recover the volume, 70 μL of 10 mM $MgCl_2$ and 1x TAE buffer was added. The recovered mixture was incubated at 35 °C for 30 min to dissolve DNA origami bundles precipitated by PEG.

Functionalizing AuNPs with DNA Strands. We slightly modified the typical protocol of previous papers[1,63,64] to obtain the bundles attached with AuNPs. The AuNP solution (5 nm in diameter, ∼90 nM, 20 mL, Sigma-Aldrich) was shaken with 8 mg of bis(p-sulfonatophenyl)phenylphosphine dihydrate dipotassium salt (BSPP, Sigma-Aldrich) at room temperature overnight. The solution was divided into 1 mL per tube, and 200 μL of 5 M NaCl was added to each tube. Then, it was shaken and centrifuged at 1700 rcf and 4 °C for 30 min. The supernatant was removed until the pellet remained only. The pellet was resuspended in 16 μL of 2.5 mM BSPP solution and 16 μL of methanol. The centrifugation of the solution and the removal of the supernatant were performed again with the same conditions. The pellet was resuspended in 16 μL of a 2.5 mM BSPP

https://doi.org/10.1021/acsnano.3c10386
ACS Nano 2024, 18, 3414−3423

solution without methanol. The concentration of the AuNPs was estimated using a NanoDrop One spectrophotometer (Thermo Fisher Scientific) by measuring the absorbance at 520 nm.

Thiolated single-stranded DNA (ssDNA) (5′-thiol-TTTTTTTTTTTTTTTTTTT-3′) was incubated with 10 mM Tris(carboxyethyl) phosphine hydrochloride (TCEP, Sigma-Aldrich) for 30 min in order to disconnect its disulfide bonds. AuNPs and thiolated ssDNA were mixed in a ratio of 1:60 (AuNP/ssDNA) in 0.5x TBE buffer (44.5 mM Tris-borate, 1 mM EDTA, Sigma-Aldrich). For salt aging, 1.5 M NaCl was added 5 times with incubation for 20 min each time to reach the final concentration of 500 mM NaCl. The final solution was incubated at room temperature overnight. To remove the excess thiolated ssDNA, we purified the solution by using a 100 kDa centrifugal filter (Amicon Ultra, Merck Millipore). The empty filter was washed first with 500 μL of 10 mM $MgCl_2$ and 1x TAE buffer at 14,000 rcf and 20 °C for 5 min. Then, 100 μL of the solution was added to the filter and washed 4 times with 400 μL of 10 mM $MgCl_2$ and 1x TAE buffer at 14,000 rcf and 20 °C for 5 min.

Assembling DNA Origami Bundles and AuNPs. We mixed purified AuNPs and DNA origami bundles at the ratio of 5 AuNPs per binding site. The mixture was incubated from 38 to 25 °C at the rate of −1 °C/h. AuNP-attached DNA origami bundles were separated from excess AuNPs through gel extraction by running the incubated mixture at 1% agarose gel in 10 mM $MgCl_2$ and 0.5x TBE buffer stained with EtBr (Thermo Fisher Scientific). The gel electrophoresis was performed at 75 V for 90 min in a bath filled with iced water. To extract the structures, the cut and chopped bands were frozen at −27 °C for 5 min. Then, they were centrifuged at 7000 rcf and 20 °C for 5 min using Freeze 'N Squeeze DNA Gel Extraction Spin Columns (Bio-Rad).

Buffer Exchange. To remove the EtBr used for gel staining from the gel-extracted samples, they were purified by using a 50 kDa centrifugal filter. The empty filter was washed with 500 μL of 15 mM $MgCl_2$ and 1x TAE buffer at 5000 rcf and 20 °C for 8 min. The washed filter was filled with the gel-extracted samples and was centrifuged again at 5000 rcf and 20 °C for 8 min. Then, we washed the filter 3 times with 450 μL of 15 mM $MgCl_2$ and 1x TAE buffer at 5000 rcf and 20 °C for 8 min followed by the recovery of samples at 10,000 rcf and 20 °C for 3 min. The recovered samples were diluted in order to achieve ∼1.0 nM structures in buffer conditions of 15 mM $MgCl_2$, 1x TAE, and a target concentration of intercalators such as EtBr, DOX, and AO (Sigma-Aldrich). Then, they were incubated at room temperature for 20 min.

Ag Enhancement. The attached AuNPs were grown using the commercial Ag enhancement kit[1] (HQ Silver, Nanoprobes, www.nanoprobes.com). The A (initiator), B (moderator), and C (activator) solutions of the kit were mixed in equal volumes and diluted with deionized (DI) water to set the absorbance at a wavelength of 290 nm to ∼200 AU. The diluted A+B+C solution (3 μL) was added to 10 μL of the buffer-exchanged sample (∼1.0 nM structures). Because the diluted A+B+C solution did not contain intercalators, the target concentration of intercalators in the sample solution should be higher than the final concentration in the previous buffer exchange process. The mixture was incubated at room temperature for 20 min without light.

AFM and TEM Measurements. Images of samples were measured by using AFM (Park NX10, Park Systems) and TEM (JEM-2100Plus, JEOL). For AFM images, 5 μL of the sample was deposited on the clean mica detached with scotch tape and incubated for 5 min. Then, it was cleaned 3 times with 200 μL of DI water and blown using a nitrogen gun. For TEM images, 10 μL of the sample was deposited on the discharged TEM grid in the negative glow and incubated for 10 min. It was washed twice with DI water and once with 2% uranyl acetate buffer. Then, the washed grid was stained with 2% uranyl acetate buffer for 40 s. After drying the grid at room temperature for 30 min, TEM images were captured at 200 kV. From the TEM images, we counted the numbers of the zigzag and non-zigzag deposition forms of AuNPs at each EtBr concentration. Then, we calculated the zigzag ratio relative to the total number of the zigzag and non-zigzag deposition forms. The standard deviation of the zigzag ratio was calculated using the bootstrapping method by repeating the process 10,000 times through the bootstrap sampling function of MATLAB (Figure S4). The diameter and gap of AuNPs and Au@Ag NPs were measured using ImageJ (https://imagej.nih.gov).

Optical Measurement. Optical signals were measured by using a CD spectrometer (Chirascan-plus, Applied Photophysics). To fill into a cuvette (104-002-10-40, Hellma Analytics, path length 10 mm), the Ag-enhanced samples were diluted with the buffer containing the target concentration of intercalators in order to set the volume of the solution to 300 μL. Then, the diluted solution was incubated at 4 °C overnight. Due to the error in the sizes of Au@Ag NPs, CD values of at least three different samples fabricated under the same conditions were measured and averaged. The contents in the buffer such as $MgCl_2$, TAE, Ag ions, and intercalators did not show CD signals at a range of concentrations (Figure S30). The g-factor (Kuhn's dissymmetry factor)[4,65−67] was calculated as follows:

$$\text{g-factor} = \frac{\epsilon_L - \epsilon_R}{(\epsilon_L + \epsilon_R)/2} = \frac{\Delta\epsilon}{\epsilon} = \frac{\text{CD [A.U.]}}{A_{\text{total}}\text{ [A.U.]}} \approx \frac{\text{CD [mdeg]}/32982}{A_{\text{total}}\text{ [A.U.]}}$$

where ϵ_L and ϵ_R are the molar extinction coefficients for the left and right circularly polarized light, respectively. $\Delta\epsilon$ is the molar circular dichroism. ϵ is the molar extinction coefficient for unpolarized light. A_{total} is the total absorbance for unpolarized light measured by the CD spectrometer in use.

Structural Simulation. We used SNUPI[39,40] to analyze the torsional deformation of DNA origami bundles. Some properties such as geometry and rigidity for simulation were used by averaging the default values of SNUPI, which are different depending on the sequences of base pairs (Table S3). The helical pitch of DNA was controlled by changing the angle between neighboring base pairs.

ASSOCIATED CONTENT

Supporting Information

The Supporting Information is available free of charge at https://pubs.acs.org/doi/10.1021/acsnano.3c10386.

Designs of DNA origami bundles; simulation analysis results of AuNP arrangement; attachment yield of AuNPs; TEM images and number of zigzag and non-zigzag deposition forms; results of control groups; diameter and gap for NPs; CD and total absorbance spectra for each condition; the g-factors according to the combination of different intercalator types; relationship between binding density and EtBr; calculation of positions binding AuNPs and twist angle; and DNA sequences of DNA origami bundles (PDF)

AUTHOR INFORMATION

Corresponding Author

Do-Nyun Kim − *Department of Mechanical Engineering, Seoul National University, Seoul 08826, Korea; Institute of Advanced Machines and Design and Institute of Engineering Research, Seoul National University, Seoul 08826, Korea;* orcid.org/0000-0003-0896-4552; Email: dnkim@snu.ac.kr

Authors

Taehwi Kim − *Department of Mechanical Engineering, Seoul National University, Seoul 08826, Korea;* orcid.org/0000-0002-5526-9440

Chanseok Lee − *Institute of Advanced Machines and Design, Seoul National University, Seoul 08826, Korea;* orcid.org/0000-0002-7969-4345

Jae Young Lee − *Institute of Advanced Machines and Design, Seoul National University, Seoul 08826, Korea;* orcid.org/0000-0002-6438-2699

https://doi.org/10.1021/acsnano.3c10386
ACS Nano 2024, 18, 3414−3423

Complete contact information is available at:
https://pubs.acs.org/10.1021/acsnano.3c10386

Author Contributions

T.K. and D.-N.K. conceived the concept and wrote the manuscript. T.K. designed and executed the experiments and simulations. T.K., C.L., and D.-N.K. analyzed the experimental results. T.K., J.Y.L., and D.-N.K. analyzed the simulated results. All authors commented on the manuscript.

Notes

The authors declare no competing financial interest.

ACKNOWLEDGMENTS

This research was supported by the National Convergence Research of Scientific Challenges (NRF-2020M3F7A1094299) and the Development of Original Technologies for the Next-Gen Vaccines for Infectious Diseases (NRF-2022M3E5F1018465) through the National Research Foundation of Korea (NRF) funded by the Ministry of Science and ICT.

REFERENCES

(1) Kuzyk, A.; Schreiber, R.; Fan, Z.; Pardatscher, G.; Roller, E.-M.; Högele, A.; Simmel, F. C.; Govorov, A. O.; Liedl, T. DNA-based Self-assembly of Chiral Plasmonic Nanostructures with Tailored Optical Response. *Nature* **2012**, *483*, 311−314.
(2) Gansel, J. K.; Thiel, M.; Rill, M. S.; Decker, M.; Bade, K.; Saile, V.; von Freymann, G.; Linden, S.; Wegener, M. Gold Helix Photonic Metamaterial As Broadband Circular Polarizer. *Science* **2009**, *325*, 1513−1515.
(3) Mark, A. G.; Gibbs, J. G.; Lee, T. C.; Fischer, P. Hybrid Nanocolloids with Programmed Three-Dimensional Shape and Material Composition. *Nat. Mater.* **2013**, *12*, 802−807.
(4) Lee, H.-E.; Ahn, H.-Y.; Mun, J.; Lee, Y. Y.; Kim, M.; Cho, N. H.; Chang, K.; Kim, W. S.; Rho, J.; Nam, K. T. Amino-Acid- and Peptide-Directed Synthesis of Chiral Plasmonic Gold Nanoparticles. *Nature* **2018**, *556*, 360−365.
(5) Kim, Y.; Yeom, B.; Arteaga, O.; Jo Yoo, S.; Lee, S.-G.; Kim, J.-G.; Kotov, N. A. Reconfigurable Chiroptical Nanocomposites with Chirality Transfer from the Macro- to the Nanoscale. *Nat. Mater.* **2016**, *15*, 461−468.
(6) Probst, P. T.; Mayer, M.; Gupta, V.; Steiner, A. M.; Zhou, Z.; Auernhammer, G. K.; König, T. A. F.; Fery, A. Mechano-Tunable Chiral Metasurfaces via Colloidal Assembly. *Nat. Mater.* **2021**, *20*, 1024−1028.
(7) George, J.; Kar, S.; Anupriya, E. S.; Somasundaran, S. M.; Das, A. D.; Sissa, C.; Painelli, A.; Thomas, K. G. Chiral Plasmons: Au Nanoparticle Assemblies on Thermoresponsive Organic Templates. *ACS Nano* **2019**, *13*, 4392−4401.
(8) Guerrero-Martínez, A.; Auguié, B.; Alonso-Gómez, J. L.; Džolić, Z.; Gómez-Graña, S.; Žinić, M.; Cid, M. M.; Liz-Marzán, L. M. Intense Optical Activity from Three-Dimensional Chiral Ordering of Plasmonic Nanoantennas. *Angew. Chem., Int. Ed.* **2011**, *50*, 5499−5503.
(9) Bagiński, M.; Tupikowska, M.; González-Rubio, G.; Wójcik, M.; Lewandowski, W. Shaping Liquid Crystals with Gold Nanoparticles: Helical Assemblies with Tunable and Hierarchical Structures via Thin-Film Cooperative Interactions. *Adv. Mater.* **2020**, *32*, e1904581.
(10) Song, C.; Blaber, M. G.; Zhao, G.; Zhang, P.; Fry, H. C.; Schatz, G. C.; Rosi, N. L. Tailorable Plasmonic Circular Dichroism Properties of Helical Nanoparticle Superstructures. *Nano Lett.* **2013**, *13*, 3256−3261.
(11) Lu, J.; Xue, Y.; Bernardino, K.; Zhang, N.-N.; Gomes, W. R.; Ramesar, N. S.; Liu, S.; Hu, Z.; Sun, T.; de Moura, A. F.; Kotov, N. A.; Liu, K. Enhanced Optical Asymmetry in Supramolecular Chiroplasmonic Assemblies with Long-Range Order. *Science* **2021**, *371*, 1368−1374.
(12) Rothemund, P. W. K. Folding DNA to Create Nanoscale Shapes and Patterns. *Nature* **2006**, *440*, 297−302.
(13) Shen, X.; Song, C.; Wang, J.; Shi, D.; Wang, Z.; Liu, N.; Ding, B. Rolling up Gold Nanoparticle-Dressed DNA Origami into Three-Dimensional Plasmonic Chiral Nanostructures. *J. Am. Chem. Soc.* **2012**, *134*, 146−149.
(14) Urban, M. J.; Dutta, P. K.; Wang, P.; Duan, X.; Shen, X.; Ding, B.; Ke, Y.; Liu, N. Plasmonic Toroidal Metamolecules Assembled by DNA Origami. *J. Am. Chem. Soc.* **2016**, *138*, 5495−5498.
(15) Liu, Y.; Ma, L.; Jiang, S.; Han, C.; Tang, P.; Yang, H.; Duan, X.; Liu, N.; Yan, H.; Lan, X. DNA Programmable Self-Assembly of Planar, Thin-Layered Chiral Nanoparticle Superstructures with Complex Two-Dimensional Patterns. *ACS Nano* **2021**, *15*, 16664−16672.
(16) Kuzyk, A.; Schreiber, R.; Zhang, H.; Govorov, A. O.; Liedl, T.; Liu, N. Reconfigurable 3D Plasmonic Metamolecules. *Nat. Mater.* **2014**, *13*, 862−866.
(17) Zhou, C.; Duan, X.; Liu, N. A Plasmonic Nanorod That Walks on DNA Origami. *Nat. Commun.* **2015**, *6*, 8102.
(18) Lan, X.; Liu, T.; Wang, Z.; Govorov, A. O.; Yan, H.; Liu, Y. DNA-Guided Plasmonic Helix with Switchable Chirality. *J. Am. Chem. Soc.* **2018**, *140*, 11763−11770.
(19) Wang, M.; Dong, J.; Zhou, C.; Xie, H.; Ni, W.; Wang, S.; Jin, H.; Wang, Q. Reconfigurable Plasmonic Diastereomers Assembled by DNA Origami. *ACS Nano* **2019**, *13*, 13702−13708.
(20) Xin, L.; Zhou, C.; Duan, X.; Liu, N. A Rotary Plasmonic Nanoclock. *Nat. Commun.* **2019**, *10*, 5394.
(21) Gür, F. N.; Kempter, S.; Schueder, F.; Sikeler, C.; Urban, M. J.; Jungmann, R.; Nickels, P. C.; Liedl, T. Double- to Single-Strand Transition Induces Forces and Motion in DNA Origami Nanostructures. *Adv. Mater.* **2021**, *33*, e2101986.
(22) Peil, A.; Zhan, P.; Duan, X.; Krahne, R.; Garoli, D.; Liz-Marzán, L. M.; Liu, N. Transformable Plasmonic Helix with Swinging Gold Nanoparticles. *Angew. Chem., Int. Ed.* **2023**, *62*, e202213992.
(23) Kuzyk, A.; Yang, Y.; Duan, X.; Stoll, S.; Govorov, A. O.; Sugiyama, H.; Endo, M.; Liu, N. A Light-Driven Three-Dimensional Plasmonic Nanosystem That Translates Molecular Motion into Reversible Chiroptical Function. *Nat. Commun.* **2016**, *7*, 10591.
(24) Jiang, Q.; Liu, Q.; Shi, Y.; Wang, Z.-G.; Zhan, P.; Liu, J.; Liu, C.; Wang, H.; Shi, X.; Zhang, L.; Sun, J.; Ding, B.; Liu, M. Stimulus-Responsive Plasmonic Chiral Signals of Gold Nanorods Organized on DNA Origami. *Nano Lett.* **2017**, *17*, 7125−7130.
(25) Kuzyk, A.; Urban, M. J.; Idili, A.; Ricci, F.; Liu, N. Selective Control of Reconfigurable Chiral Plasmonic Metamolecules. *Sci. Adv.* **2017**, *3*, e1602803.
(26) Huang, Y.; Nguyen, M.-K.; Natarajan, A. K.; Nguyen, V. H.; Kuzyk, A. A DNA Origami-Based Chiral Plasmonic Sensing Device. *ACS Appl. Mater. Interfaces* **2018**, *10*, 44221−44225.
(27) Zhou, C.; Xin, L.; Duan, X.; Urban, M. J.; Liu, N. Dynamic Plasmonic System That Responds to Thermal and Aptamer-Target Regulations. *Nano Lett.* **2018**, *18*, 7395−7399.
(28) Man, T.; Ji, W.; Liu, X.; Zhang, C.; Li, L.; Pei, H.; Fan, C. Chiral Metamolecules with Active Plasmonic Transition. *ACS Nano* **2019**, *13*, 4826−4833.
(29) De Fazio, A. F.; Misatziou, D.; Baker, Y. R.; Muskens, O. L.; Brown, T.; Kanaras, A. G. Chemically Modified Nucleic Acids and DNA Intercalators As Tools for Nanoparticle Assembly. *Chem. Soc. Rev.* **2021**, *50*, 13410−13440.
(30) Ryssy, J.; Natarajan, A. K.; Wang, J.; Lehtonen, A. J.; Nguyen, M.-K.; Klajn, R.; Kuzyk, A. Light-Responsive Dynamic DNA-Origami-Based Plasmonic Assemblies. *Angew. Chem.* **2021**, *60*, 5923−5927.
(31) Kim, Y.-J.; Lee, C.; Lee, J. G.; Kim, D.-N. Configurational Design of Mechanical Perturbation for Fine Control of Twisted DNA Origami Structures. *ACS Nano* **2019**, *13*, 6348−6355.
(32) Ono, A.; Cao, S.; Togashi, H.; Tashiro, M.; Fujimoto, T.; Machinami, T.; Oda, S.; Miyake, Y.; Okamoto, I.; Tanaka, Y. Specific

Interactions between Silver(I) Ions and Cytosine-Cytosine Pairs in DNA Duplexes. *Chem. Commun.* **2008**, 4825−4827.
(33) Kondo, J.; Tada, Y.; Dairaku, T.; Hattori, Y.; Saneyoshi, H.; Ono, A.; Tanaka, Y. A Metallo-DNA Nanowire with Uninterrupted One-Dimensional Silver Array. *Nat. Chem.* **2017**, *9*, 956−960.
(34) Joshi, A. S.; Singh, P.; Mijakovic, I. Interactions of Gold and Silver Nanoparticles with Bacterial Biofilms: Molecular Interactions behind Inhibition and Resistance. *Int. J. Mol. Sci.* **2020**, *21*, 7658.
(35) Chen, H.; Zhang, H.; Pan, J.; Cha, T.-G.; Li, S.; Andreasson, J.; Choi, J. H. Dynamic and Progressive Control of DNA Origami Conformation by Modulating DNA Helicity with Chemical Adducts. *ACS Nano* **2016**, *10*, 4989−4996.
(36) Li, R.; Chen, H.; Lee, H.; Choi, J. H. Conformational Control of DNA Origami by DNA Oligomers, Intercalators and UV Light. *Methods Protoc.* **2021**, *4*, 38.
(37) Kim, Y.-J.; Park, J.; Lee, J. Y.; Kim, D.-N. Programming Ultrasensitive Threshold Response through Chemomechanical Instability. *Nat. Commun.* **2021**, *12*, 5177.
(38) Lee, C.; Kim, Y.-J.; Kim, K. S.; Lee, J. Y.; Kim, D.-N. Modulating the Chemo-Mechanical Response of Structured DNA Assemblies through Binding Molecules. *Nucleic Acids Res.* **2021**, *49*, 12591−12599.
(39) Lee, J. Y.; Lee, J. G.; Yun, G.; Lee, C.; Kim, Y.-J.; Kim, K. S.; Kim, T. H.; Kim, D.-N. Rapid Computational Analysis of DNA Origami Assemblies at Near-Atomic Resolution. *ACS Nano* **2021**, *15*, 1002−1015.
(40) Lee, J. G.; Kim, K. S.; Lee, J. Y.; Kim, D.-N. Predicting the Free-Form Shape of Structured DNA Assemblies from Their Lattice-Based Design Blueprint. *ACS Nano* **2022**, *16*, 4289−4297.
(41) Nguyen, L.; Dass, M.; Ober, M. F.; Besteiro, L. V.; Wang, Z. M.; Nickel, B.; Govorov, A. O.; Liedl, T.; Heuer-Jungemann, A. Chiral Assembly of Gold-Silver Core-Shell Plasmonic Nanorods on DNA Origami with Strong Optical Activity. *ACS Nano* **2020**, *14*, 7454−7461.
(42) Cherstvy, A. G. Electrostatic Interactions in Biological DNA-Related Systems. *Phys. Chem. Chem. Phys.* **2011**, *13*, 9942−9968.
(43) Fischer, S.; Hartl, C.; Frank, K.; Rädler, J. O.; Liedl, T.; Nickel, B. Shape and Interhelical Spacing of DNA Origami Nanostructures Studied by Small-Angle X-ray Scattering. *Nano Lett.* **2016**, *16*, 4282−4287.
(44) Sayed, M.; Krishnamurthy, B.; Pal, H. Unraveling the Salt Induced Modulation in the Photophysical Behavior of Acridine Orange Dye on Its Interaction with Natural DNA. *J. Mol. Liq.* **2021**, *336*, 116146.
(45) Wang, J. G. The Degree of Unwinding of the DNA Helix by Ethidium. I. Titration of Twisted PM2 DNA Molecules in Alkaline Cesium Chloride Density Gradients. *J. Mol. Biol.* **1974**, *89*, 783−801.
(46) Jones, R. L.; Lanier, A. C.; Keel, R. A.; Wilson, W. D. The Effect of Ionic Strength on DNA-Tigand Unwinding Angles for Acridine and Quinoline Derivatives. *Nucleic Acids Res.* **1980**, *8*, 1613−1624.
(47) Waring, M. J. DNA Modification and Cancer. *Annu. Rev. Biochem.* **1981**, *50*, 159−192.
(48) Welch, J. J.; Rauscher, F. J., 3rd; Beerman, T. A. Targeting DNA-binding Drugs to Sequence-Specific Transcription Factor.DNA Complexes. Differential Effects of Intercalating and Minor Groove Binding Drugs. *J. Biol. Chem.* **1994**, *269*, 31051−31058.
(49) Lyles, M. B.; Cameron, I. L. Interactions of the DNA Intercalator Acridine Orange, with Itself, with Caffeine, and with Double Stranded DNA. *Biophys. Chem.* **2002**, *96*, 53−76.
(50) Alonso, A.; Almendral, M. J.; Curto, Y.; Criado, J. J.; Rodríguez, E.; Manzano, J. L. Determination of the DNA-Binding Characteristics of Ethidium Bromide, Proflavine, and Cisplatin by Flow Injection Analysis: Usefulness in Studies on Antitumor Drugs. *Anal. Biochem.* **2006**, *355*, 157−164.
(51) Tartakoff, S. S.; Finan, J. M.; Curtis, E. J.; Anchukaitis, H. M.; Couture, D. J.; Glazier, S. Investigations into the DNA-Binding Mode of Doxorubicinone. *Org. Biomol. Chem.* **2019**, *17*, 1992−1998.
(52) Lee, C.; Kim, K. S.; Kim, Y.-J.; Lee, J. Y.; Kim, D.-N. Tailoring the Mechanical Stiffness of DNA Nanostructures Using Engineered Defects. *ACS Nano* **2019**, *13*, 8329−8336.
(53) Lee, J. Y.; Kim, M.; Lee, C.; Kim, D.-N. Characterizing and Harnessing the Mechanical Properties of Short Single-Stranded DNA in Structured Assemblies. *ACS Nano* **2021**, *15*, 20430−20441.
(54) Chen, Y.; Yang, X.; Gao, J. Spin-Controlled Wavefront Shaping with Plasmonic Chiral Geometric Metasurfaces. *Light Sci. Appl.* **2018**, *7*, 84.
(55) Chen, C.; Gao, S.; Song, W.; Li, H.; Zhu, S.-N.; Li, T. Metasurfaces with Planar Chiral Meta-Atoms for Spin Light Manipulation. *Nano Lett.* **2021**, *21*, 1815−1821.
(56) Kim, J.; Rana, A. S.; Kim, Y.; Kim, I.; Badloe, T.; Zubair, M.; Mehmood, M. Q.; Rho, J. Chiroptical Metasurfaces: Principles, Classification, and Applications. *Sensors* **2021**, *21*, 4381.
(57) Kershner, R. J.; Bozano, L. D.; Micheel, C. M.; Hung, A. M.; Fornof, A. R.; Cha, J. N.; Rettner, C. T.; Bersani, M.; Frommer, J.; Rothemund, P. W. K.; Wallraff, G. M. Placement and Orientation of Individual DNA Shapes on Lithographically Patterned Surfaces. *Nat. Nanotechnol.* **2009**, *4*, 557−561.
(58) Hung, A. M.; Micheel, C. M.; Bozano, L. D.; Osterbur, L. W.; Wallraff, G. M.; Cha, J. N. Large-Area Spatially Ordered Arrays of Gold Nanoparticles Directed by Lithographically Confined DNA Origami. *Nat. Nanotechnol.* **2010**, *5*, 121−126.
(59) Gopinath, A.; Miyazono, E.; Faraon, A.; Rothemund, P. W. K. Engineering and Mapping Nanocavity Emission via Precision Placement of DNA Origami. *Nature* **2016**, *535*, 401−405.
(60) Gopinath, A.; Thachuk, C.; Mitskovets, A.; Atwater, H. A.; Kirkpatrick, D.; Rothemund, P. W. K. Absolute and Arbitrary Orientation of Single-Molecule Shapes. *Science* **2021**, *371*, eabd6179.
(61) Douglas, S. M.; Marblestone, A. H.; Teerapittayanon, S.; Vazquez, A.; Church, G. M.; Shih, W. M. Rapid Prototyping of 3D DNA-Origami Shapes with CaDNAno. *Nucleic Acids Res.* **2009**, *37*, 5001−5006.
(62) Wagenbauer, K. F.; Engelhardt, F. A. S.; Stahl, E.; Hechtl, V. K.; Stömmer, P.; Seebacher, F.; Meregalli, L.; Ketterer, P.; Gerling, T.; Dietz, H. How We Make DNA Origami. *ChemBioChem.* **2017**, *18*, 1873−1885.
(63) Gür, F. N.; Schwarz, F. W.; Ye, J.; Diez, S.; Schmidt, T. L. Toward Self-Assembled Plasmonic Devices: High-Yield Arrangement of Gold Nanoparticles on DNA Origami Templates. *ACS Nano* **2016**, *10*, 5374−5382.
(64) Wang, P.; Huh, J.-H.; Lee, J.; Kim, K.; Park, K. J.; Lee, S.; Ke, Y. Magnetic Plasmon Networks Programmed by Molecular Self-Assembly. *Adv. Mater.* **2019**, *31*, 1901364.
(65) Woody, R. W. Circular Dichroism. In *Methods in Enzymology*; Sauer, K., Ed.; Academic Press: Boston, MA, 1995; pp 34−71.
(66) McPhie, P. Circular Dichroism Studies on Proteins in Films and in Solution: Estimation of Secondary Structure by G-Factor Analysis. *Anal. Biochem.* **2001**, *293*, 109−119.
(67) Baker, B. R.; Garrell, R. L. G-Factor Analysis of Protein Secondary Structure in Solutions and Thin Films. *Faraday Discuss.* **2004**, *126*, 209−222.

https://doi.org/10.1021/acsnano.3c10386
ACS Nano 2024, 18, 3414−3423